Application of transthoracic shear-wave ultrasound elastography in lung lesions

Yao-Wen Kuo[1], Yen-Lin Chen[2], Huey-Dong Wu[1], Ying-Chun Chien[2], Chun-Kai Huang[2] and Hao-Chien Wang[2,3]

Affiliations: [1]Dept of Integrated Diagnostics and Therapeutics, National Taiwan University Hospital, Taipei, Taiwan. [2]Dept of Internal Medicine, National Taiwan University Hospital, Taipei, Taiwan. [3]Dept of Medicine, National Taiwan University Cancer Center, Taipei, Taiwan.

Correspondence: Hao-Chien Wang, Dept of Medicine, National Taiwan University Cancer Center, No. 57, Lane 155, Section 3, Keelung Road, Taipei 106, Taiwan. E-mail: haochienwang@gmail.com

@ERSpublications
Transthoracic shear-wave ultrasound elastography can help in differentiating malignant from benign subpleural lung lesions. Tissue proofing should be considered in pulmonary hypoechoic or air bronchogram lesions with high elasticity. https://bit.ly/3liKvBr

Cite this article as: Kuo Y-W, Chen Y-L, Wu H-D, *et al.* Application of transthoracic shear-wave ultrasound elastography in lung lesions. *Eur Respir J* 2021; 57: 2002347 [https://doi.org/10.1183/13993003.02347-2020].

ABSTRACT

Introduction: Tissue stiffness information may help in the diagnosis of lung lesions. This study aimed to investigate and validate the application of transthoracic two-dimensional shear-wave ultrasound elastography in differentiating malignant from benign subpleural lung lesions.

Methods: This study involved one retrospective observational derivation cohort from January 2016 to December 2017 and one prospective observational validation cohort from December 2017 to December 2019. The inclusion criterion was radiographic evidence of pulmonary lesions. The patients were categorised into air bronchogram and hypoechoic groups based on B-mode grayscale images. The elasticity of subpleural lung lesions with acceptable shear-wave propagation was measured. Diagnoses were made on the basis of pathology, microbiological studies or following up the clinical course for at least 6 months.

Results: A total of 354 patients were included. Among the 121 patients in the derivation cohort, a receiver operating characteristic curve was constructed and the cut-off point to differentiate benign from malignant lesions was 65 kPa with a Youden index of 0.60 and an accuracy of 84.3%. Among the 233 patients in the validation cohort, the diagnostic performance was maintained, with a Youden index of 0.65 and an accuracy of 86.7%. Upon applying the cut-off point to the air bronchogram group, the Youden index was 0.70 and the accuracy was 85.0%.

Conclusions: This study validated the application of transthoracic shear-wave ultrasound elastography for assessing lung malignancy. A cut-off point of 65 kPa is suggested for predicting lung malignancy. Furthermore, for pulmonary air bronchogram lesions with high elasticity, tissue proofing should be considered because of the high possibility of malignancy.

This article has an editorial commentary: https://doi.org/10.1183/13993003.04260-2020

This article has supplementary material available from erj.ersjournals.com

This study is registered at ClinicalTrials.gov with identifier number NCT03376425. Individual deidentified participant data including the data dictionaries, study protocol and statistical analysis plan will be shared immediately following publication with no end date. The data will be shared with researchers who provide a methodologically sound proposal to achieve aims in the approved proposal. Proposals should be directed to the corresponding author.

Received: 16 June 2020 | Accepted: 28 Sept 2020

Introduction

Advancements in imaging capacities and the development of a precise puncture-guiding transducer have made transthoracic ultrasonography a useful diagnostic tool for evaluating peripheral subpleural lung tumours [1, 2]. Ultrasound-guided transthoracic real-time needle aspiration biopsy (UTNAB) has proved to be a reliable and safe diagnostic modality in several thoracic diseases [3]. Nevertheless, the heterogeneity of lung malignancy with necrosis may limit the accuracy of UTNAB. For lung malignancy that mimics pneumonia on chest radiographs and ultrasound images, tissue proofing is typically not considered until the failure of empirical antibiotic treatment [4].

Different human tissues have varying levels of elasticity because of the properties of the extracellular matrix [5]. Ultrasound elastography has been intensively employed to image the liver, thyroid, breast, prostate, kidney, lymph nodes and musculoskeletal diseases with promising results [6–12]. In pulmonology, Izumo *et al.* [13] used endobronchial ultrasound elastography to predict mediastinal and hilar nodal metastases. Pleural two-dimensional (2D) shear-wave elastography (SWE) can be used to differentiate between malignant pleural effusion and benign pleural disease [14–16]. For subpleural lung lesions, high shear-wave velocity was observed in lung malignancy compared with benign lung lesions by point SWE or acoustic radiation force impulse elastography [17, 18]. Lim *et al.* [19] deployed transthoracic ultrasonography strain elastography with external manual compression to image lung lesions. The strain ratio of necrosis was low, whereas the strain ratio of primary lung cancer was significantly higher than that of pneumonia.

Transthoracic 2D-SWE uses acoustic radiation force and assesses the velocity of tissue displacement propagation in multiple focal zones. The shear waves are monitored in 2D by creating a near-cylindrical shear-wave cone, enabling measurement of the shear-wave speed or Young's modulus (E) on a colour quantitative elastogram [20]. Based on the hypothesis that transthoracic 2D-SWE could add accurate tissue stiffness information to B-mode grayscale ultrasound images and help in differentiating lung malignancy from benign lung lesions, this study aimed to investigate and validate the predictive value of transthoracic 2D-SWE in the diagnosis of subpleural lung lesions.

Methods

Study design

This study employed one retrospective observational derivation cohort from January 2016 to December 2017 and one observational validation cohort including consecutive prospectively enrolled patients from December 2017 to December 2019. The inclusion criterion was radiographic evidence of pulmonary lesions. The exclusion criteria were age <20 years and an inability to hold breath for at least 5 s. This study was conducted at the chest ultrasound unit in a tertiary medical centre (National Taiwan University Hospital, Taipei, Taiwan). Written informed consent was obtained from each patient or surrogate in the prospective validation cohort before examinations (ClinicalTrials.gov identifier number NCT03376425).

Chest ultrasound and 2D-SWE

We used an Aplio 500 Platinum ultrasound machine (Toshiba Medical Systems, Tochigi-Ken, Japan) with a convex transducer (1.5–6 MHz; Aplio PVT-375BT) for chest ultrasound examinations. First, we used the B-mode grayscale images of subpleural lung lesions to categorise the patients into air bronchogram and hypoechoic groups. The air bronchogram group was defined by tubular hyperechoic artefacts within the lung lesion and a serrated margin with reverberation echoes at the margin. The hypoechoic group referred to lung lesions without any tubular hyperechoic artefacts. Information on size, location and intercostal chest wall thickness was collected. We then asked the patient to hold their breath for 5 s and simultaneously began the transthoracic 2D-SWE measurement. On propagation display, the shear-wave arrival time was presented as contour lines. Only after obtaining adequate shear-wave propagation in at least certain regions of the lesion did we switch to the elasticity and speed displays. We used regions of interest (ROIs) with 3 mm diameter and selected up to four ROIs with the highest mean elasticity values. The elasticity measurements were performed one time in the derivation cohort and three times in the validation cohort. We calculated the average as the final value (refer to the supplementary material for the protocol of SWE and supplementary figures E1–E3). If patients had multiple subpleural lung lesions, we chose the largest and most approachable lesion to perform 2D-SWE. In patients who consented to undergo UTNAB after transthoracic SWE, UTNAB was performed if the lesion was approachable and the risks of bleeding and pneumothorax were low.

Data collection

Baseline characteristics of patients (including age, sex and body mass index) were collected. Final diagnoses were obtained using one of the following three methods: 1) pathology or cytology per UTNAB,

bronchoscopic biopsy, computed tomography (CT)-guided biopsy or surgical operation, 2) microbiological studies and 3) following up the clinical course for 6 months after the chest ultrasound studies.

Benign lesions were classified as bacterial pneumonia, tuberculosis, fungal pneumonia and others. Bacterial pneumonia was defined on the basis of clinical presentations and results of microbiological studies or referring the lung lesions that resolved after antibiotic use. Malignant lesions were classified as lung adenocarcinoma, small cell lung carcinoma (SCLC), squamous cell lung carcinoma, nonsmall cell lung carcinoma not otherwise specified (NSCLC-NOS), metastatic lung cancer, lymphoma and others.

Safety

We reviewed the patients' medical records and follow-up chest radiography to see if haemoptysis or pneumothorax developed during or after chest ultrasound examinations. At our chest ultrasound unit, we routinely use ultrasound to evaluate the presence of lung point sign, stratosphere sign or loss of gliding at the end of the UTNAB, followed by chest radiography to detect any pneumothorax.

Inter-rater reliability

The chest ultrasound examinations (including B-mode and 2D-SWE) were performed by two pulmonologists (raters) with >5 years of experience in chest ultrasonography. The two raters were blinded to the diagnosis of the lesion. To assess the inter-rater reliability, we randomly selected 11 patients in the validation cohort and the 2D-SWE measurements of their lung lesions were performed by each rater.

Statistics

Data are presented as mean with standard deviation or median (interquartile range (IQR)) for continuous measures and number (percentage) for categorical measures. The baseline characteristics of the derivation and validation cohorts were compared using the Pearson Chi-squared test or t-test. The derivation cohort was used to construct a receiver operating characteristic (ROC) curve. The cut-off point was determined by maximising the Youden function to differentiate malignant from benign lung lesions. The cut-off point was then used to construct 2×2 contingency tables comparing the disease status (malignant/benign based on the final diagnoses) to the SWE results (positive/negative based on cut-off point dichotomy). Diagnostic performance of SWE was assessed using sensitivity, specificity, positive predictive value, negative predictive value, accuracy, positive likelihood ratio and negative likelihood ratio. The derivation and validation cohorts were combined to conduct a multiple logistic regression model to determine the probability of lung malignancy after adjusting for age, sex and possible confounding covariates. Inter-rater reliability was expressed by the Pearson product–moment correlation coefficient (r). Box plots were used to illustrate the distribution of the elasticity value among different aetiologies in benign and malignant lung lesions, and the difference in elasticity was investigated using one-way ANOVA on rank. The ROC curve was plotted using MedCalc version 13.0.6.0 (MedCalc, Ostend, Belgium). The other statistics were obtained using Stata version 14.0 (StataCorp, College Station, TX, USA). All tests of significance were two-sided, with $p<0.05$ indicating statistical significance.

Results

Patients' characteristics

Figure 1 presents a flowchart of patient enrolment from January 2016 to December 2019. Overall, 586 consecutive patients with radiographic evidence of pulmonary lesions were screened and 471 patients underwent transthoracic 2D-SWE. Unacceptable shear-wave propagation was observed in 65 patients (supplementary table E1) and no definite diagnoses could be made in 24 patients. Finally, 354 patients were included in the analyses, with 121 patients in the derivation cohort and 233 patients in the validation cohort. The clinical characteristics of patients in the derivation and validation cohorts are presented in table 1. Among the 354 patients, mean±SD age was 65.3±13.5 years and most patients (61.3%) were male; mean±SD body mass index (BMI) was 22.6±3.8 $kg \cdot m^{-2}$ and lung lesion size was 49.7±26.4 mm. The location of lung lesions was: right upper lobe 27.1%, right lower lobe 25.4%, left lower lobe 21.8%, left upper lobe 18.9% and right middle lobe 6.8%. Most lung lesions were malignant (68.6%) and hypoechoic (77.4%). The baseline characteristics were comparable between the two cohorts except for the lower intercostal chest wall thickness in the derivation cohort (17.8 *versus* 19.7 mm; p=0.004).

Among the 243 patients with diagnosis of lung malignancy, six patients did not undergo UTNAB and diagnoses could not be discerned using UTNAB of the lungs in 20 patients. Hence, the diagnoses in these 26 patients were made later through bronchoscopic biopsy (n=9), CT-guided lung biopsy (n=7), biopsy of nonlung tissue (n=6), surgical biopsy (n=3) and sputum cytology (n=1). Among the 111 patients with a diagnosis of benign lung lesions, 65 patients underwent UTNAB. The diagnoses were made by pathology (n=21), microbiological study (n=22) and clinical course (n=68).

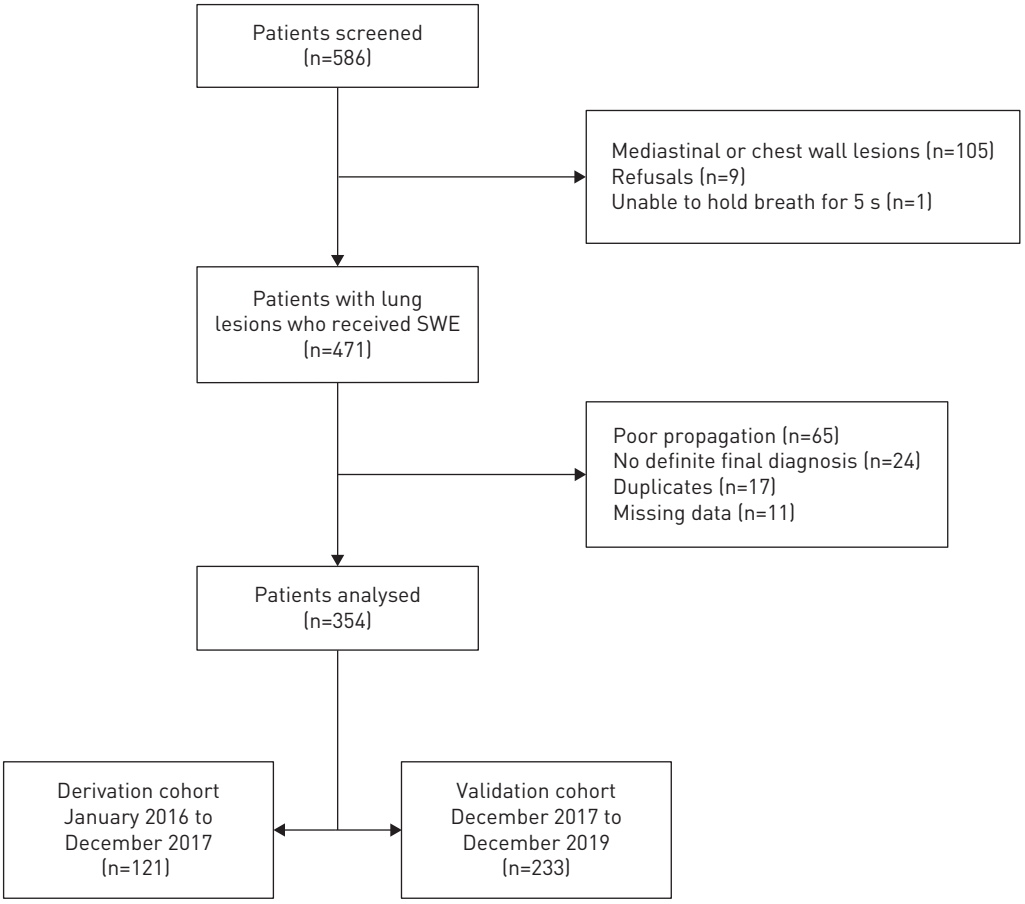

FIGURE 1 Flowchart of patient enrolment from January 2016 to December 2019. SWE: shear-wave elastography.

Diagnostic performance of 2D-SWE

The derivation cohort was used to determine the optimal cut-off point. Figure 2 reveals that a cut-off point of 65 kPa resulted in the maximal Youden index (0.60) for differentiating between benign and malignant lesions (sensitivity 89.7%, specificity 70.6%, accuracy 84.3% and area under the ROC curve 0.866; p<0.001). The diagnostic performance was maintained when using the same cut-off point in the validation cohort (accuracy 86.7% and Youden index 0.65). When applying the cut-off point to the air bronchogram group, the Youden index was 0.70 and the accuracy was 85.0% (table 2).

Elasticity among different aetiologies of lung lesions

Figure 3 illustrates the distribution of elasticity values among benign and malignant lesions. Bacterial and fungal pneumonia constituted most of the benign lesions, and the median (IQR) elasticity was 42.64 (22.77–57.45) and 54.33 (33.03–65.73) kPa, respectively. The median (IQR) elasticity among patients with tuberculosis was 77.53 (71.29–89.10) kPa, which was higher than the cut-off point of 65 kPa. Significant differences were observed between various types of benign lesions (p=0.013) (figure 3a). Lung adenocarcinoma constituted a major portion of the lung malignancy observed in this study, with a median (IQR) elasticity of 103.09 (92.20–113.98) kPa. A wide range of elasticity values was obtained in patients with SCLC (median (IQR) 95.09 (69.28–105.36) kPa). The median (IQR) elasticity of metastatic lung cancer and lung lymphoma was 105.22 (94.29–122.76) and 109.09 (98.22–120.97) kPa, respectively. No significant difference was observed between the different types of malignant lesions (p=0.201) (figure 3b). Representative examples of 2D-SWE images are presented in supplementary figure E4.

In the air bronchogram group, 59 patients had benign lung lesions and 21 had malignant lung lesions. The median (IQR) elasticity of bacterial pneumonia (n=39), fungal pneumonia (n=9), tuberculosis (n=6) and adenocarcinoma (n=13) was 38.24 (20.00–53.73), 35.41 (30.08–52.83), 72.62 (38.65–82.18) and 93.75 (77.83–103.04) kPa, respectively.

TABLE 1 Clinical characteristics of the derivation and validation cohorts

	Total	Derivation cohort	Validation cohort	p-value
Patients	354	121	233	
Age years	65.3±13.5	63.6±13.0	66.2±13.7	0.082
Male	217 (61.3)	79 (65.3)	138 (59.2)	0.267
BMI kg·m^{-2}	22.6±3.8	22.5±3.7	22.7±3.8	0.744
Lung lesion size mm	49.7±26.4	50.3±25.3	49.4±27.0	0.756
Intercostal chest wall thickness mm	19.0±6.1	17.8±5.2	19.7±6.4	0.004
Location				0.313
Right upper lobe	96 (27.1)	27 (22.3)	69 (29.6)	
Right middle lobe	24 (6.8)	10 (8.3)	14 (6.0)	
Right lower lobe	90 (25.4)	30 (24.8)	60 (25.8)	
Left upper lobe	67 (18.9)	29 (24.0)	38 (16.3)	
Left lower lobe	77 (21.8)	25 (20.7)	52 (22.3)	
Aetiology				0.341
Benign	111 (31.4)	34 (28.1)	77 (33.0)	
Bacterial pneumonia	62 (17.5)	13 (10.7)	49 (21.0)	
Tuberculosis	13 (3.7)	9 (7.4)	4 (1.7)	
Fungal pneumonia	23 (6.5)	9 (7.4)	14 (6.0)	
Others[#]	13 (3.7)	3 (2.5)	10 (4.3)	
Malignant	243 (68.6)	87 (71.9)	156 (67.0)	
ADC	120 (33.9)	44 (36.4)	76 (32.6)	
SCLC	23 (6.5)	8 (6.6)	15 (6.4)	
SqCC	32 (9.0)	5 (4.1)	27 (11.6)	
NSCLC-NOS	25 (7.1)	9 (7.4)	16 (6.9)	
MLC	20 (5.6)	10 (8.3)	10 (4.3)	
Lymphoma	8 (2.3)	4 (3.3)	4 (1.7)	
Others[¶]	15 (4.2)	7 (5.8)	8 (3.4)	
B-mode ultrasound image				0.86
Hypoechoic	274 (77.4)	93 (76.9)	181 (77.7)	
Air bronchogram	80 (22.6)	28 (23.1)	52 (22.3)	

Data are presented as n, mean±SD or n (%), unless otherwise stated. BMI: body mass index; ADC: adenocarcinoma; SCLC: small cell lung carcinoma; SqCC: squamous cell carcinoma; NSCLC-NOS: nonsmall cell lung carcinoma not otherwise specified; MLC: metastatic lung cancer. [#]: other benign lesions included nine patients in whom the lung lesions subsided spontaneously without definite treatment, two patients with IgG4-related lung disease, one patient with organising pneumonia and one patient with calcifying fibrous tumour; [¶]: other malignant lesions included four patients with spindle cell carcinoma, three patients with lymphoepithelioma-like carcinoma, three patients with sarcomatoid carcinoma, two patients with pleomorphic carcinoma, one patient with epithelioid haemangioendothelioma, one patient with Ewing sarcoma and one patient with combined SCLC/ADC.

In the hypoechoic group, 52 patients had benign lung lesions and 222 had malignant lung lesions. The median (IQR) elasticity of bacterial pneumonia (n=23), fungal pneumonia (n=14) and tuberculosis (n=7) was 56.50 (26.94–93.30), 62.51 (54.33–94.12) and 85.43 (76.85–122.93) kPa, respectively. The median (IQR) elasticity of adenocarcinoma (n=107), SCLC (n=23), squamous cell lung carcinoma (n=29), NSCLC-NOS (n=24) and metastatic lung cancer (n=19) was 103.74 (94.19–114.61), 95.09 (69.28–105.36), 104.53 (92.81–112.63), 103.37 (86.99–110.64) and 106.55 (93.78–127.43) kPa, respectively.

Determination of the independent predictive factors of lung malignancy

Age, sex and factors significantly associated with lung malignancy in univariable analyses ($p \leqslant 0.05$) were included in the multivariable analysis (supplementary table E2). Age, lung lesion size, B-mode ultrasound image (hypoechoic *versus* air bronchogram) and elasticity >65 kPa were the independent predictors of lung malignancy (OR 1.04 (95% CI 1.01–1.07), 1.03 (95% CI 1.02–1.05), 5.72 (95% CI 2.60–12.59) and 20.11 (95% CI 9.33–43.32), respectively).

Safety

A total of 471 patients underwent transthoracic 2D-SWE. Among the 386 patients undertaking UTNAB after 2D-SWE measurements, 12 patients (3.1%) developed mild post-biopsy haemoptysis and another nine patients (2.3%) developed post-biopsy pneumothorax. No pneumothorax or haemoptysis was observed among the 85 patients undertaking 2D-SWE measurements only.

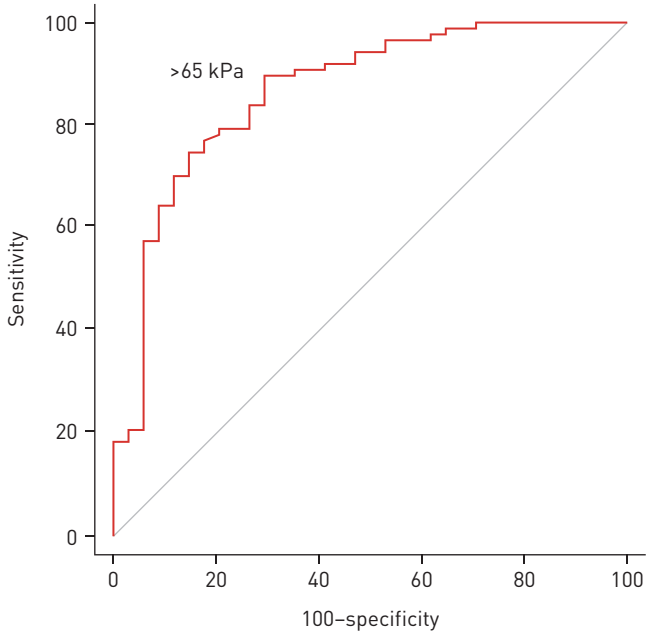

FIGURE 2 Receiver operating characteristic (ROC) curve based on the derivation cohort (n=121). The optimal cut-off point of 65 kPa for predicting lung malignancy is shown (Youden index 0.60, sensitivity 89.7%, specificity 70.6% and area under the ROC curve 0.866; p<0.001).

Inter-rater reliability

Regarding inter-rater reliability, two raters evaluated the SWE in a subset of 11 randomly selected patients based on the standardised operating protocol in the validation cohort. A strong correlation was discovered between the elasticity values given by the two raters (r=0.93; p<0.001). Besides these 11 chest ultrasound examinations, rater 1 interpreted 248 examinations and rater 2 interpreted 95 examinations.

Discussion

This study investigates and validates the predictive value of transthoracic 2D-SWE in differentiating malignant from benign subpleural lung lesions. The cut-off point suggested in this study is 65 kPa. To the best of our knowledge, this is the first study to have validated the application of transthoracic 2D-SWE in the diagnosis of lung lesions.

Transthoracic 2D-SWE quantitatively reveals tissue stiffness and is less operator dependent compared with strain elastography [19, 21]. In this study, the shear-wave propagation display served as a quality control tool to measure elasticity reliably. We did not record the elasticity value if no adequate shear-wave propagation could be observed within the lesions. Besides rapid onsite cytopathological examination and colour Doppler ultrasound imaging [22–24], transthoracic 2D-SWE can add tissue stiffness information to B-mode grayscale ultrasound images and may be used as an adjunctive tool with UTNAB, bronchoscopy and CT-guided biopsy if tissue proofing is indicated. Another clinical implication of SWE is that it can help in assessing lung malignancy mimicking pneumonia and nonresolving consolidation [25]. Chest sonography of these patients may reveal a consolidation lesion with air bronchogram and pulmonary vasculatures. UTNAB might be deferred because of concern over haemoptysis from vascular injury. Pneumonic-type lung adenocarcinoma and non-Hodgkin lymphoma may involve lung parenchyma

TABLE 2 Diagnostic performance of cut-off point (>65 kPa) in predicting malignant lesions in different cohorts and groups

	Patients n	Sensitivity %	Specificity %	PPV %	NPV %	Accuracy %	LR+	LR–
Cohort								
Derivation	121	89.7 (81.3–95.2)	70.6 (52.5–84.9)	88.6 (80.1–94.4)	72.7 (54.5–86.7)	84.3 (76.6–90.3)	3.05 (1.80–5.16)	0.15 (0.08–0.28)
Validation	233	94.9 (90.1–97.8)	70.1 (58.6–80.0)	86.6 (80.5–91.3)	87.1 (76.1–94.3)	86.7 (81.6–90.8)	3.18 (2.25–4.48)	0.07 (0.04–0.15)
Group								
Air bronchogram	80	85.7 (63.7–97.0)	84.8 (73.0–92.8)	66.7 (46.0–83.5)	94.3 (84.3–98.8)	85.0 (75.3–92.0)	5.62 (3.00–10.50)	0.17 (0.06–0.48)
Hypoechoic	274	93.7 (89.6–96.5)	53.9 (39.5–67.8)	89.7 (85.0–93.3)	66.7 (50.5–80.4)	86.1 (81.5–90.0)	2.03 (1.51–2.73)	0.12 (0.07–0.21)

Numbers in parentheses represent 95% CI. PPV: positive predictive value; NPV: negative predictive value; LR+: positive likelihood ratio; LR–: negative likelihood ratio.

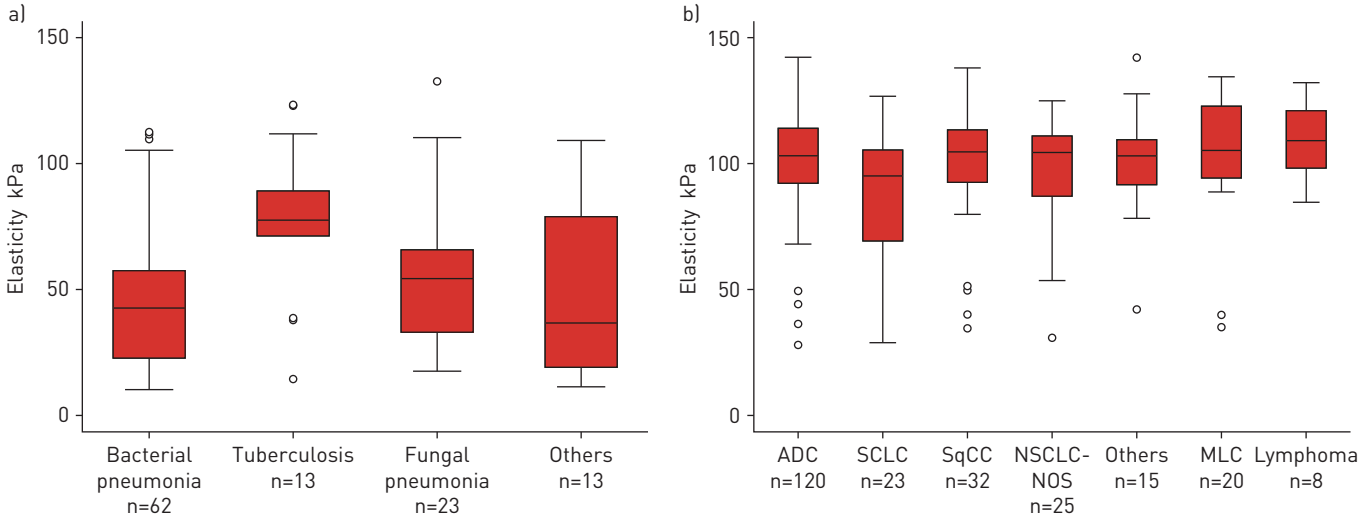

FIGURE 3 Box plot showing elasticity of the different benign (n=111) and malignant lung lesions (n=243): a) a significant difference was noted between different types of benign lesions (p=0.013), b) whereas no significant difference was discovered between different types of malignant lesions (p=0.201). ADC: adenocarcinoma; SCLC: small cell lung carcinoma; SqCC: squamous cell carcinoma; NSCLC-NOC: nonsmall cell lung carcinoma not otherwise specified; MLC: metastatic lung cancer. Box plots show median and interquartile range (IQR); whiskers represent 1.5 IQR and outliers are indicated.

without obstruction of a bronchus, present with pneumonia-like consolidations and lead to diagnostic delays [26–28]. For pulmonary air bronchogram lesions with high elasticity, tissue proofing should be considered because of the high possibility of malignancy.

The safety issue of SWE has been raised since acoustically induced techniques require push pulses to displace the local tissues [29–31]. In this study, no haemoptysis or pneumothorax was observed among the 85 patients undertaking 2D-SWE measurements without biopsy. Among the 386 patients undertaking UTNAB after 2D-SWE measurements, the rate of post-biopsy haemoptysis was 3.1% and the rate of post-biopsy pneumothorax was 2.3%. Compared with the previous cohort study at our chest ultrasound unit with 6% post-biopsy haemoptysis and 4% post-biopsy pneumothorax [32], the risk of post-biopsy complications did not increase after 2D-SWE measurements. Nevertheless, the full safety profile of 2D-SWE for the lung needs further investigation.

Notably, acute bacterial infection had lower elasticity than chronic tuberculosis infection. 10 out of 13 patients with tuberculosis in this study had elasticity higher than the cut-off point of 65 kPa, causing false-positive results. This problem was also reported in a study using SWE for assessing tuberculous pleurisy [14]. This finding is probably because of tubercles conglomerating into a firm lump or an irregular thick wall in pulmonary tuberculosis [33]. The elasticity of SCLC in this study was relatively low (median 95.09 kPa) and had a wide range (IQR 69.28–105.36 kPa). The extensive necrotic nature of SCLC may result in this finding [34].

To differentiate lung malignancy from benign lung lesions, Wei *et al.* [18] used point SWE and selected 1.951 $m \cdot s^{-1}$ as the cut-off shear-wave velocity, whereas Ozgokce *et al.* [17] found the optimal cut-off value was 2.47 $m \cdot s^{-1}$. The cut-off points of 1.951 or 2.47 $m \cdot s^{-1}$ (~11 or 18 kPa) were lower than the cut-off of 65 kPa obtained in this study. However, the techniques of point SWE and 2D-SWE are different [20, 35]. Point SWE uses acoustic radiation force to induce tissue displacement in a single focal location, whereas 2D-SWE allows monitoring of shear waves in multiple focal zones. Up to four ROIs in each SWE measurement were assessed in this study. The strengths of this 2D-SWE study are its large sample, the validation method, and the selection of ROIs on the basis of the B-mode and shear-wave propagation map.

This study had some limitations. First, although the propagation mode could serve as a quality measurement map to help select the ROI, some techniques are mandatory to obtain adequate measurement of SWE, including obtaining the optimal B-mode image, avoiding excessive tissue compression by the transducer, and the correct instruction to patients to hold their breath during the specific respiratory phase to ensure the lung lesion is perpendicular to the probe and simultaneously avoid rib shadowing. Second, some signal void areas were observed in 2D-SWE. This observation was probably because of the heterogeneity within the lung lesion, intralesional necrosis or the existence of liquid within

the lesion [35]. Therefore, to avoid obtaining such areas, an ROI diameter of 3 mm was applied in this study. Furthermore, the doctors performing the UTNAB were not necessarily aware of the elastogram and, hence, the ROI locations were not necessarily the biopsy areas. Third, pulsation of the heart or great vessels, thick chest walls, or presence of pleural effusion interfered with the transthoracic SWE of 65 patients (13.8%), causing unacceptable shear-wave propagations (supplementary figure E5). Fourth, the relatively low to normal BMI and thin intercostal chest wall thickness in this study may place additional limits on the generalisation to other populations of overweight and obese patients. Moreover, the applicability of transthoracic SWE is limited to peripheral subpleural lung lesions. Finally, this study had a relatively small number of patients with benign lesions or in the air bronchogram group. In most clinical scenarios at our hospital, the doctor arranges a chest ultrasound examination if the clinical suspicion of lung malignancy is high. Therefore, the high incidence of lung malignancy in a tertiary medical centre could have affected the positive and negative predictive values.

In conclusion, this study demonstrated and validated the excellent performance of transthoracic 2D-SWE in differentiating between malignant and benign subpleural lung lesions. Additional study to compare the diagnostic yield of SWE-guided and conventional UTNAB for subpleural lung lesions is warranted to further investigate the predictive value of 2D-SWE.

Author contributions: Y-W. Kuo and H-C. Wang contributed to the study design, acquisition, analysis and interpretation of the data, and drafted the manuscript. Y-L. Chen, H-D. Wu, Y-C. Chien and C-K. Huang contributed to the acquisition, analysis or interpretation of the data. All authors contributed to the critical revision of the manuscript for important intellectual content.

Conflict of interest: None declared.

Support statement: This work was financially supported by the Ministry of Science and Technology in Taiwan (107-2314-B-002-234). Funding information for this article has been deposited with the Crossref Funder Registry.

References

1 Tsai TH, Yang PC. Ultrasound in the diagnosis and management of pleural disease. *Curr Opin Pulm Med* 2003; 9: 282–290.
2 Yang P. Applications of colour Doppler ultrasound in the diagnosis of chest diseases. *Respirology* 1997; 2: 231–238.
3 Yang PC. Ultrasound-guided transthoracic biopsy of the chest. *Radiol Clin North Am* 2000; 38: 323–343.
4 Low DE, Mazzulli T, Marrie T. Progressive and nonresolving pneumonia. *Curr Opin Pulm Med* 2005; 11: 247–252.
5 Riegler J, Labyed Y, Rosenzweig S, *et al.* Tumor elastography and its association with collagen and the tumor microenvironment. *Clin Cancer Res* 2018; 24: 4455–4467.
6 Ferraioli G, Parekh P, Levitov AB, *et al.* Shear wave elastography for evaluation of liver fibrosis. *J Ultrasound Med* 2014; 33: 197–203.
7 Lin P, Chen M, Liu B, *et al.* Diagnostic performance of shear wave elastography in the identification of malignant thyroid nodules: a meta-analysis. *Eur Radiol* 2014; 24: 2729–2738.
8 Liu B, Zheng Y, Huang G, *et al.* Breast lesions: quantitative diagnosis using ultrasound shear wave elastography – a systematic review and meta-analysis. *Ultrasound Med Biol* 2016; 42: 835–847.
9 Lupsor-Platon M, Badea R, Gersak M, *et al.* Noninvasive assessment of liver diseases using 2D shear wave elastography. *J Gastrointestin Liver Dis* 2016; 25: 525–532.
10 Jiao Y, Dong F, Wang H, *et al.* Shear wave elastography imaging for detecting malignant lesions of the liver: a systematic review and pooled meta-analysis. *Med Ultrason* 2017; 19: 16–22.
11 Ryu J, Jeong WK. Current status of musculoskeletal application of shear wave elastography. *Ultrasonography* 2017; 36: 185–197.
12 Suh CH, Choi YJ, Baek JH, *et al.* The diagnostic performance of shear wave elastography for malignant cervical lymph nodes: a systematic review and meta-analysis. *Eur Radiol* 2017; 27: 222–230.
13 Izumo T, Sasada S, Chavez C, *et al.* Endobronchial ultrasound elastography in the diagnosis of mediastinal and hilar lymph nodes. *Jpn J Clin Oncol* 2014; 44: 956–962.
14 Jiang B, Li XL, Yin Y, *et al.* Ultrasound elastography: a novel tool for the differential diagnosis of pleural effusion. *Eur Respir J* 2019; 54: 1802018.
15 Ozgokce M, Durmaz F, Yavuz A, *et al.* Shear-wave elastography in the characterization of pleural effusions. *Ultrasound Q* 2019; 35: 164–168.
16 Porcel JM. Ultrasound-based elastography: "hard" to implement in the pleural effusion work-up? *Eur Respir J* 2019; 54: 1901587.
17 Ozgokce M, Yavuz A, Akbudak I, *et al.* Usability of transthoracic shear wave elastography in differentiation of subpleural solid masses. *Ultrasound Q* 2018; 34: 233–237.
18 Wei H, Lu Y, Ji Q, *et al.* The application of conventional US and transthoracic ultrasound elastography in evaluating peripheral pulmonary lesions. *Exp Ther Med* 2018; 16: 1203–1208.
19 Lim CK, Chung CL, Lin YT, *et al.* Transthoracic ultrasound elastography in pulmonary lesions and diseases. *Ultrasound Med Biol* 2017; 43: 145–152.
20 Sigrist RMS, Liau J, Kaffas AE, *et al.* Ultrasound elastography: review of techniques and clinical applications. *Theranostics* 2017; 7: 1303–1329.
21 Gennisson JL, Deffieux T, Fink M, *et al.* Ultrasound elastography: principles and techniques. *Diagn Interv Imaging* 2013; 94: 487–495.
22 Hsu WH, Ikezoe J, Chen CY, *et al.* Color Doppler ultrasound signals of thoracic lesions. Correlation with resected histologic specimens. *Am J Respir Crit Care Med* 1996; 153: 1938–1951.

23 Wang HC, Yu CJ, Chang DB, *et al.* Transthoracic needle biopsy of thoracic tumours by a colour Doppler ultrasound puncture guiding device. *Thorax* 1995; 50: 1258–1263.
24 Liao WY, Jerng JS, Chen KY, *et al.* Value of imprint cytology for ultrasound-guided transthoracic core biopsy. *Eur Respir J* 2004; 24: 905–909.
25 Arab T, Malekzadegan MR, Morante J, *et al.* Nonresolving pneumonia in the setting of malignancy. *Curr Opin Pulm Med* 2019; 25: 331–335.
26 Wislez M, Massiani MA, Milleron B, *et al.* Clinical characteristics of pneumonic-type adenocarcinoma of the lung. *Chest* 2003; 123: 1868–1877.
27 Detterbeck FC, Marom EM, Arenberg DA, *et al.* The IASLC Lung Cancer Staging Project: background data and proposals for the application of TNM staging rules to lung cancer presenting as multiple nodules with ground glass or lepidic features or a pneumonic type of involvement in the forthcoming Eighth Edition of the TNM Classification. *J Thorac Oncol* 2016; 11: 666–680.
28 Bligh MP, Borgaonkar JN, Burrell SC, *et al.* Spectrum of CT findings in thoracic extranodal non-Hodgkin lymphoma. *Radiographics* 2017; 37: 439–461.
29 Miller DL, Dong Z, Dou C, *et al.* Pulmonary capillary hemorrhage induced by acoustic radiation force impulse shear wave elastography in ventilated rats. *J Ultrasound Med* 2019; 38: 2575–2587.
30 Saftoiu A, Gilja OH, Sidhu PS, *et al.* The EFSUMB Guidelines and Recommendations for the Clinical Practice of Elastography in Non-Hepatic Applications: Update 2018. *Ultraschall Med* 2019; 40: 425–453.
31 Kollmann C, Jenderka KV, Moran CM, *et al.* EFSUMB Clinical Safety Statement for Diagnostic Ultrasound (2019 revision). *Ultraschall Med* 2020; 41: 387–389.
32 Liao WY, Chen MZ, Chang YL, *et al.* US-guided transthoracic cutting biopsy for peripheral thoracic lesions less than 3 cm in diameter. *Radiology* 2000; 217: 685–691.
33 Bomanji JB, Gupta N, Gulati P, *et al.* Imaging in tuberculosis. *Cold Spring Harb Perspect Med* 2015; 5: a017814.
34 Travis WD. Update on small cell carcinoma and its differentiation from squamous cell carcinoma and other non-small cell carcinomas. *Mod Pathol* 2012; 25: Suppl. 1, S18–S30.
35 Bouchet P, Gennisson JL, Podda A, *et al.* Artifacts and technical restrictions in 2D shear wave elastography. *Ultraschall Med* 2020; 41: 267–277.